AGU PUBLICATIONS

Geophysical Research Letters

RESEARCH LETTER
10.1002/2016GL068829

Key Points:
- We apply a spatiotemporal spectral diagnostics to the new centennial reanalyses
- The low coverage of data before WWII seems to generate a suppression of high-frequency variability
- The assimilation of surface observations can be sufficient to generate high-quality upper air fields

Supporting Information:
- Supporting Information S1

Correspondence to:
A. Dell'Aquila,
alessandro.dellaquila@enea.it

Citation:
Dell'Aquila, A., S. Corti, A. Weisheimer, H. Hersbach, C. Peubey, P. Poli, P. Berrisford, D. Dee, and A. Simmons (2016), Benchmarking Northern Hemisphere midlatitude atmospheric synoptic variability in centennial reanalysis and numerical simulations, *Geophys. Res. Lett.*, *43*, doi:10.1002/2016GL068829.

Received 3 NOV 2015
Accepted 4 MAY 2016
Accepted article online 7 MAY 2016

Benchmarking Northern Hemisphere midlatitude atmospheric synoptic variability in centennial reanalysis and numerical simulations

Alessandro Dell'Aquila[1], Susanna Corti[2], Antje Weisheimer[3,4], Hans Hersbach[4], Carol Peubey[4], Paul Poli[4,5], Paul Berrisford[4], Dick Dee[4], and Adrian Simmons[4]

[1]ENEA, Climate & Impact Modeling Laboratory, Roma, Italy, [2]Istituto di Scienze dell'Atmosfera e del Clima, Consiglio Nazionale delle Ricerche, Bologna, Italy, [3]Department of Physics, National Centre for Atmospheric Science, University of Oxford, Oxford, United Kingdom, [4]European Centre for Medium-Range Weather Forecasts, Reading, United Kingdom, [5]Météo-France, CMM, Brest, France

Abstract The representation of midlatitude winter atmospheric synoptic variability in centennial reanalysis products, which assimilate surface observations only, and atmospheric model simulations constrained by observation-based data sets is assessed. Midlatitude waves activity in twentieth century reanalyses (20CR, ERA-20C) and atmospheric model simulations are compared with those estimated from observationally complete reanalysis products. All reanalyses are in good agreement regarding the representation of the synoptic variability during the last decades of the twentieth century. This suggests that the assimilation of surface observations can generate high-quality extratropical upper air fields. In the first decades of the twentieth century a suppression of high-frequency variability is apparent in the centennial reanalysis products. This behavior does not have a counterpart in the atmospheric model integrations. Since the latter differ from one of the reanalysis products considered here (ERA-20C) only in the assimilation of surface observations, it seems reasonable to attribute the high-frequency variability suppression to the poor coverage of the observations assimilated.

1. Introduction

The need for a "best product" climate reanalysis suitable for climate model validation and climate variability assessment over time scales ranging from days to decades has increased considerably. The many changes in the observing system since the beginning of instrumental records has resulted in most reanalyses concentrating on the "well-observed" period since 1979, with the availability of many satellite and in situ observing systems. However, reasonable quality can also be achieved by reanalyses in the Northern Hemisphere since the International Geophysical Year 1957–1958, with the generalization of routine exchange of upper air sounding observations [e.g., *Uppala et al*., 2005; *Kistler et al*., 2001]. However, these are relatively short time periods for comparison with historical climate simulations and do not cover several prominent climate events in the first half of the twentieth century.

Indeed, recently two twentieth century reanalysis products have been realised. They represent the first attempt to produce a four-dimensionally complete multivariate historical reconstruction of the global weather of the twentieth century. They are the NOAA Twentieth Century Reanalysis (20CR) produced by *Compo et al.* [2011] and the ERA-20C deterministic reanalysis carried out by the European Centre for Medium-Range Weather Forecasts in the framework of the ERA-CLIM project [*Poli et al*., 2015]. As an initial step toward comprehensive reanalyses, both products limit the observational input to surface data, with the explicit intent in 20CR that this choice may result in improved product consistency during the century. On the other hand, this limitation in the observation input affects the accuracy of these products for recent times with respect to reanalysis that assimilates surface, upper air, and satellite observations. However, studies using advanced data assimilation methods (e.g., 4-D-Var and ensemble Kalman filter) have suggested that the surface network could be used to generate high-quality upper air fields [e.g., *Thépaut*, 2006, *Whitaker et al*., 2009; *Compo et al*., 2006]. *Poli et al.* [2013, 2015] have shown that this notion is especially applicable to the midlatitude and high latitude where reanalyses obtained by assimilating only surface pressure observations may reproduce fairly well the daily evolution of tropospheric meteorology.

In the light of these considerations, the 20CR and ERA-20C reanalyses seem particularly suitable for studying decadal variations in the main features of extratropical synoptic atmospheric variability. In particular our analysis focuses on high and low atmospheric variability as represented by propagating and standing waves defined following the spatiotemporal spectral decomposition firstly introduced by *Hayashi* [1971, 1979] and here applied in the formulation of *Fraedrich and Bottger* [1978] (see supporting information). The representation of midlatitude atmospheric variability and the associated underlying processes such as the baroclinic conversion of available energy [*Blackmon,* 1976; *Speranza,* 1983] and the interaction of planetary waves with the orography [*Charney and De Vore*, 1979; *Charney and Straus,* 1980] could be of importance even in the context of long-term projections where changes in atmospheric variability at different time scales could modify the frequency of high impact events such as, for example, heat waves and extreme precipitation.

In this context we adopt the process-oriented metrics for planetary and baroclinic waves described in *Di Biagio et al.* [2014] to compare different reanalysis products and ERA-20CM model simulations carried out in the framework of the ERA-CLIM project [*Hersbach et al*., 2015].

2. Data and Methodology

Four data sets, covering the period from 1900 to 2010, are analyzed in terms of their capability of simulating the wintertime northern Hemisphere midlatitude synoptic atmospheric variability. They consist of: (i) the deterministic reanalysis ERA-20C; (ii) 20CR; (iii) ERA-20CM; (iv) modified model simulations with stochastic physics (hereafter ERA-20CM-SP). The last two which differ in that ERA-20CM-SP applies stochastic perturbations to the physical tendencies [*Palmer et al*., 2009; *Weisheimer et al*., 2014] whereas ERA-20CM does not, and ERA-20CM-SP consists of 3 ensemble members instead of 10 for ERA-20CM. However, for sake of consistency and fair comparison, here we consider only those three ensemble members of ERA-20CM forced by the same realizations of the Hadley centre sea Ice and Sea-Surface Temperature data set (HadISST) data set [*Rayner et al*., 2003] used for the correspondent ensemble members in ERA-20CM-SP. It is worth mentioning that the two centennial reanalyses considered here present some differences in the way they were produced as well as in the data assimilated. The deterministic reanalysis ERA-20C is produced by a unique run assimilating surface-only observations (namely, surface and mean sea level pressures and surface marine winds), employing a four-dimensional variational (4-D-Var) analysis scheme [*Poli et al*., 2015]. On the other hand, 20CR is obtained by 56-member Kalman filter ensemble runs assimilating only surface/mean sea level pressure. For this study we have here considered the 20CR ensembles mean, freely available in the NOAA ftp server. All the data sets are compared in the most recent period, with the most observationally complete reanalysis products available, such as National Centers for Environmental Prediction (NCEP)-National Center for Atmospheric Research (NCAR) [*Kistler et al*., 2001], ERA-40 [*Uppala et al*., 2005], and ERA-Interim [*Dee et al*., 2011].

The wintertime synoptic midlatitude atmospheric variability is studied here by adopting a process-oriented metric based on the spatiotemporal Hayashi spectral decomposition [*Di Biagio et al*., 2014; *Lucarini et al*., 2007; *Dell'Aquila et al*., 2005] applied to the December-January-February (DJF) daily 500 hPa geopotential height data averaged over the latitudinal belt 30°N–75°N, where most of the baroclinic and the low-frequency wave activity is observed [*Dell'Aquila et al*., 2005] (Further details about Hayashi technique are reported in the supporting information). Since the data were produced at different horizontal resolutions, to homogenize the outputs, all data sets have been interpolated on the same grid, namely, the coarsest one at $2.5 \times 2.5°$ (NCEP-NCAR, ERA-40). We focus on eastward propagating high-frequency waves along with standing (i.e., characterized by fixed spatial nodes/antinodes) low-frequency waves. The good agreement between different reanalysis products such as NCEP-NCAR, ERA-40, and ERA-Interim in terms of the representation of atmospheric variability has been shown and widely discussed in previous studies [e.g., *Dell'Aquila et al*., 2005, *Lucarini et al*., 2007; *Di Biagio et al*., 2014]. Therefore, we can use the NCEP-NCAR reanalysis as reference for the second half of 20th and the first decade of the 21st centuries. The climatological averages of Hayashi spectra for DJF from NCEP-NCAR are in fairly good agreement with those computed from ERA-20C, ERA-20CM, and ERA-20CM-SP for the (overlapping) period 1979–2010 (see Figures S1 and S2 in the supporting information).

The consistency of Hayashi spectra between the different datasets leads to a common definition of spectral subdomains for the integral metric of the energy associated to propagating and standing waves. The energy $\boldsymbol{H_E}$ of the synoptic eastward traveling waves, i.e., waves associated with the release of available energy driven

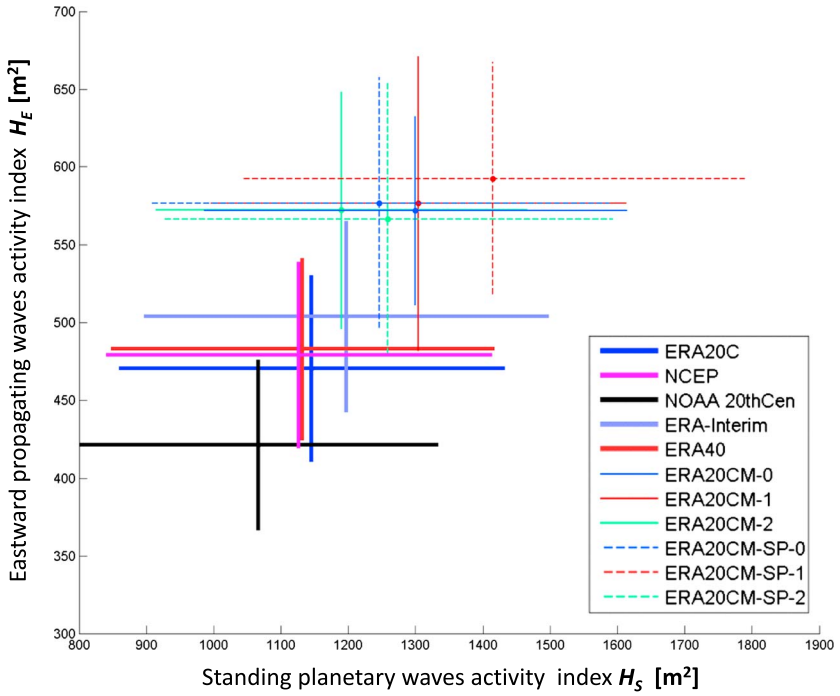

Figure 1. Scatterplot of index of eastward propagating waves activity H_E (*y* axis), versus the index of the planetary standing waves activity H_S (*x* axis), computed for the *Z* 500 hPa DJF data averaged in the latitudinal belt 30°N–75°N for the overlapping period 1979–2001. The bars stand for ±1 temporal standard deviation. The thick lines are for the reanalysis data sets. The thin solid lines are for the ERA20CM runs, while the dashed lines are for the corresponding ERA20CM-SP runs with the effects of Stochastic Physics included.

by conventional baroclinic conversion [*Blackmon*, 1976; *Speranza*, 1983; *Wallace et al*., 1983], is computed by integrating over each winter season the eastward propagating component of power spectrum over the high-frequency high-wavenumber (i.e., zonal wavenumbers larger than 6, with period 2–7 days) spectral domain. On the other hand, the planetary scale energy H_S, mostly interacting with orography [*Charney and De Vore*, 1979; *Charney and Straus*, 1980; *Benzi et al*., 1986] and catalyzed by the subtropical jet [*Benzi and Speranza*, 1989; *Ruti et al*., 2006], is computed by integrating the standing component of the power spectrum over the low-frequency low-wavenumber spectral domain, corresponding to 10–45 days and zonal wavenumbers between 2 and 4. The choice of these spectral subdomains is based on the results reported in recent literature (see *Di Biagio et al*. [2014], *Lucarini et al*. [2007], and *Dell'Aquila et al*. [2005] for major details). In the next section the quantities H_E and H_S will be used as global indices to represent respectively the behavior of baroclinic and planetary wave energy.

3. Results

Figure 1 shows a scatterplot of the integral values for H_E and H_S averaged over the common overlapping period 1979–2001 for DJF from the different data sets. Horizontal (vertical) error bars represent the standard deviation (taken here as a measure of interannual variability) of the annual values of H_E (H_S). The thick lines refer to reanalysis products, the thin lines are for members 0, 1, and 2 of ERA-20CM simulations, while the dashed lines describe the corresponding ERA-20CM-SP simulations. (It is worth remarking that member 0 of each simulation uses the same realization of the HadISST data set adopted for the ERA-20C reanalysis.)

Reanalysis products appear in good agreement for both the mean value and interannual variability (error bars) with the only, partial, exception represented by 20CR, which systematically underestimates baroclinic (*y* axis) and planetary scale (*x* axis) activity. This is expected, considering that 20CR is an ensemble mean and therefore could smooth the Z500 hPa field and reduce its variability. On the other hand, ERA-20CM and ERA-20CM-SP products exhibit a systematic, nonnegligible, overestimation of wave activity and related interannual variability. This result is particularly remarkable considering that the ERA-20C reanalysis was produced using the same cycle of Integrated

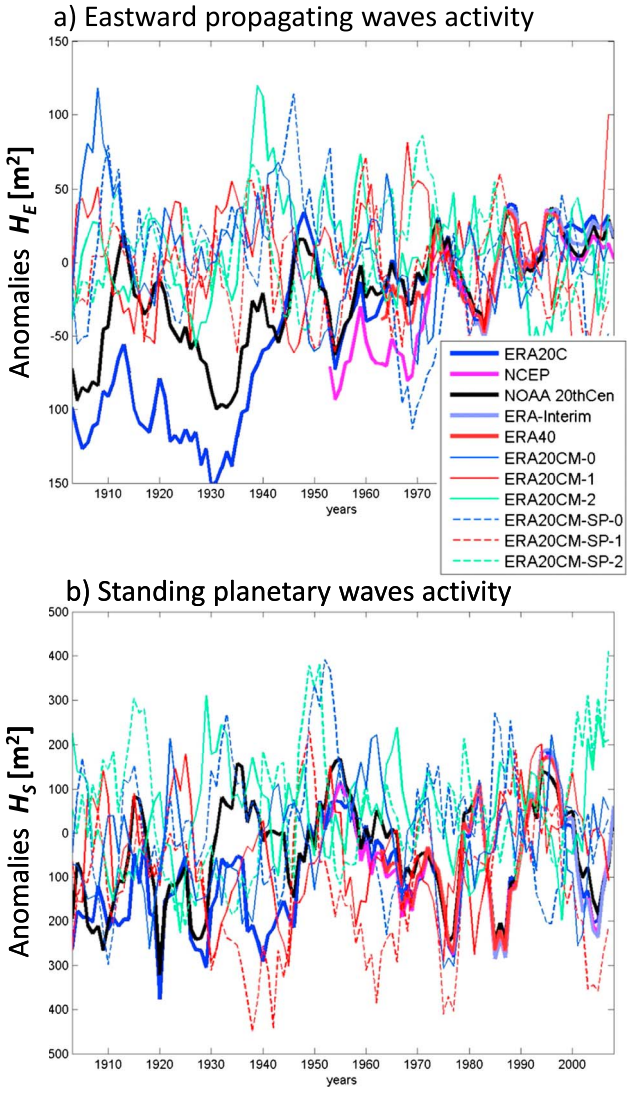

Figure 2. Time series of the anomalies (with respect to 1979–2001 period) of (a) index of eastward propagating waves activity H_E and (b) index of the planetary standing waves activity H_S, in the latitudinal belt 30°N–75°N, by the ERA20C, NCEP, NOAA 20th CEN, ERA-Interim, ERA40, and ERA-CLIM ERA20CM, ERA20CM-SP. We apply a 5 year running mean.

Forecasting System (IFS) model used to perform the ERA-20CM (ERA-20CM-SP) simulations. The inclusion of stochastic physics does affect the low-frequency long waves; however, the relative changes are not consistent among the three ensemble members. In two cases (green and red ensemble members) we can recognize an increase of H_S for ERA-20CM-SP, while, for the blue ensemble member, stochastic physics seems to contribute to a decrease of H_S. However, it is worth noting that these differences are lower than the interannual variability of the index. These results are independent on the specific time period used to compute the integral values of H_E (and H_S).

In Figure 2 the time series of H_E (a) and H_S (b) for the DJF anomalies with respect to the mean values reported in Figure 1 are displayed. Since the year-to-year variability is considerable, a 5 year running mean has been applied. For both indices, the time evolution since 1979 is in good agreement between all reanalyses products (thick curves). This supports the notion that the assimilation of only surface fields can be sufficient to generate high-quality upper air synoptic variability for the extratropical belt during the winter season. It is interesting to note that H_E, the index related to baroclinic activity, exhibits a slight positive trend from the 1970s, while the index of planetary wave activity, H_S, displays pronounced decadal variations but no trend. Interannual and decadal variations in H_S are consistent among different reanalyses also during the first quarter of the second half of the twentieth century (i.e., when the observation coverage is more limited). Some differences can be noted in the same period for H_E time series, with NCEP-NCAR showing lower wave activities than other products. An evident suppression of baroclinic waves activity occurs in the first 40 years of the two twentieth century historical reanalyses: ERA-20C (blue curve) and 20CR (black curve). This suppression of variability in the early decades appears much stronger in ERA-20C than in 20CR. However, one should take into account that for the period 1979-2001 20CR shows a reduction in H_E and H_S of the order of 50 m^2, compared to the other reanalyses (Figure 1). In fact the time series of the full values (Figure S3) show a similar (reduced) baroclinic wave activity for 20CR and ERA-20C before 1940. The lower values of H_E in the early decades of the century do not have a counterpart in the model simulations ERA-20CM (thin curves) and ERA-20CM-SP (dashed curves). The latter exhibits no trend but pronounced oscillations consistent with the values of standard deviation reported in Figure 1. It is worth recalling here that ERA-20C, ERA-20CM, and ERA-20CM-SP are forced by the same, CMIP5-protocol-recommended, radiative forcing [*Taylor et al*., 2012] and the same sea surface boundary conditions. ERA-20C does assimilate surface observations, while in the latter two products the model is free to produce its own variability. Similar (but not identical)

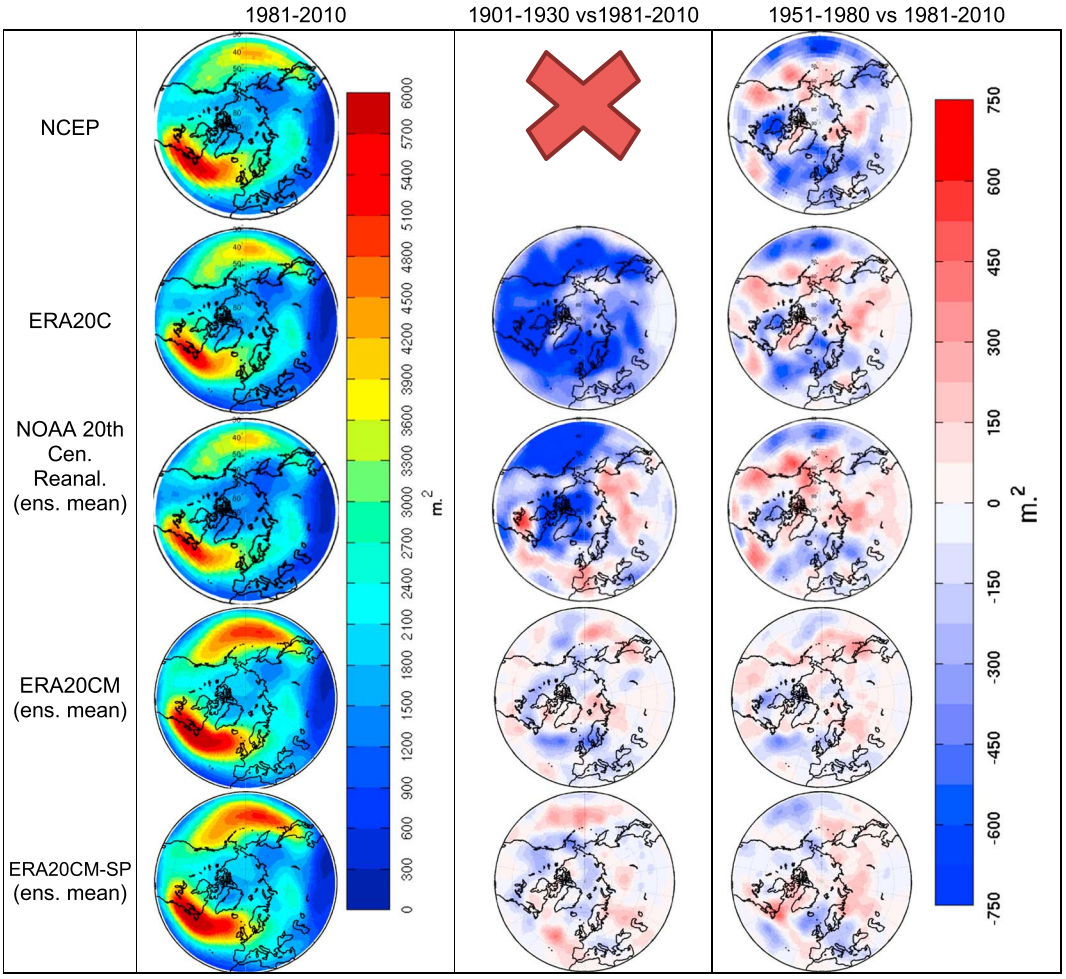

Figure 3. Maps of 2–7 days band-pass variance of 500 hPa geopotential height for different periods and different data sets: we report as reference the variance for (left column) 1981–2010 DJF period. The changes of period (middle column) 1901–1930 and (right column) 1951–1980 with respect to reference period 1981–2010. For ERA20CM (-SP) we report the results pertaining to the ensemble mean.

features are also evident in the H_S time series, where ERA-20C and 20CR show a suppression of wave activity during the first 30–40 years of the century.

The changes in the H_E index observed in the first decades of the twentieth century are consistent with more conventional analyses of atmospheric high-frequency variability. For example, in Figure 3, we show the maps of the 2–7 day DJF band-pass variance of 500 hPa geopotential height computed in different 30 year periods for NCEP-NCAR, ERA-20C, 20CR, ERA-20CM, and ERA-20CM-SP data sets. In Figure 3 (left column) the high-frequency variance for the period 1981–2010 is displayed. (For ERA-20CM and ERA-20CM-SP, Figure 3 also shows the mean variance computed over the first three ensemble members.) The three reanalysis data sets exhibit quite similar patterns, while, consistently with the results shown in Figure 1, model simulations overestimate the 2–7 day variance both in the Atlantic and, to a larger extent, in the Pacific storm track regions. In Figure 3 (middle and right columns) we report the difference between the maps in Figure 3 (left column), i.e., the high-frequency variance of 500 hPa geopotential height and the same for the periods 1901–1930 and 1951–1980, respectively. The systematic underestimation of high-frequency variability in the first 30 years of the twentieth century in ERA-20C and in 20CR is apparent. In ERA-20C the high-frequency variability suppression extends to the whole latitudinal band, while in the 20CR reanalysis this is mostly confined to the Pacific sector. Consistently with the time series shown in Figure 2, different 30 year periods are characterized by a pronounced variability in the mean 2–7 day DJF band-pass variance in the model simulations. However, none of the maps shown in Figure 3 exhibits a global suppression of variability as that found in ERA-20C and

20CR in the period 1901–1930. This conclusion is valid also when single ensemble members are considered: within the ensemble of six members we cannot find differences between two 30 year periods comparable with those found in ERA-20C between 1981–2010 and 1901–1930.

The maps displayed in Figure 3 (left column) report the changes in high-frequency variability in the second half of the twentieth century (i.e., 1951–1980 versus 1981–2010). As noted above, during the second part of the century the different reanalysis products considered here are highly consistent. They all show in the period 1951–1980 reduced high-frequency variability over the oceanic storm track regions and a northward migration of these disturbances in the Pacific sector. These features apply also to the difference pattern of ERA-20CM; however, the magnitude of anomalies is smaller. When the stochastic physics is included (ERA-20CM-SP), the signal changes sign in the Pacific North American region and over the Atlantic subploar gyre. Similar outcomes, but somehow weaker, are found for the low-frequency atmospheric variability (which is related to $\boldsymbol{H_S}$, the index for standing planetary waves) during the same 30 year periods. In the ERA-20C and 20CR reanalyses the 500 hPa geopotential height 10–45 day band-pass variance is very low compared to the 1981–2010 period. Again, this signal does not have a counterpart in the model simulations (see Figure S4 in the supporting information).

4. Concluding Remarks

A process-oriented metric has been used to assess the capability of century long reanalysis products (ERA-20C and 20CR) and model simulations (ERA-20CM and ERA-20CM-SP) in reproducing the wintertime northern Hemisphere midlatitude synoptic atmospheric variability. We focus on high-frequency propagating disturbances (baroclinic waves, with a time scale shorter than 7 days) and on low-frequency planetary waves (time scale longer than 10 days).

In the recent period (1979–2010), ERA-20C exhibits a good agreement in the representation of variability on both time scales when compared with observationally complete reanalysis products such as ERA-Interim, ERA-40, and NCEP-NCAR (see Figure 1), supporting the notion that in the extratropical band, the assimilation of surface variables, can be sufficient to generate high-quality upper air fields [*Poli et al*., 2013]. In the same period the ensemble mean of 20CR underestimates $\boldsymbol{H_E}$ and $\boldsymbol{H_S}$ by about 10%. Model simulations (ERA-20CM and ERA-20CM-SP), on the other hand, show a nonnegligible and systematic overestimation of wave activity and the related interannual variability. This applies in particular to the high-frequency propagating disturbances, with all the ensemble members showing consistent behavior. The inclusion of stochastic physics affects the longwave index $\boldsymbol{H_S}$, leading to an increase of the average values of $\boldsymbol{H_S}$ for two out of three ensemble members.

The spatial distribution of high-frequency and low-frequency wintertime extratropical variability in the 30 year period 1981–2010 is fairly consistent between the different reanalyses and model simulations (see Figures 3 and S4). However, the latter overestimate the high-frequency variability over the Atlantic and Pacific storm tracks. Reduced high-frequency variability over the oceanic storm track regions is found in the previous 30 years (1951–1980) in the reanalyses and, partially, in both sets of model simulations. In the reanalyses this signal translates into a positive trend shown by the $\boldsymbol{H_E}$ index over the second half of twentieth century (see Figure 2). A similar trend cannot be found in any of ERA-20CM and ERA-20CM-SP simulations. In fact, in the latter the magnitude of the anomalies shown in Figure 3 is much smaller (indicating that there is a modest consistency between the different ensemble members). Anomalies in ERA-20CM are in general agreement with those found in ERA-20CM-SP, with the exceptions of the Pacific North American and the Atlantic subpolar gyre regions, where they exhibit opposite sign.

In the first four decades of the century a clear suppression of high-frequency variability is apparent both in ERA-20C and 20CR (see Figures 2 and 3). The same kind of signal, but weaker, is found for the low-frequency variability in the same period. High- and low-frequency variability in ERA-20CM and ERA-20CM-SP simulations do not show a similar dramatic change of variability, either in the same period or in any other 30 year periods. Since ERA-20CM and ERA-20CM-SP integrations differ from ERA-20C reanalysis only in the assimilation of surface observations, it seems reasonable to attribute the suppression of high-frequency variability in the first decades of the twentieth century in ERA-20C to the poor coverage of the observations assimilated. In this respect it is worth noting that the number of observations from land (ship) stations assimilated in ERA-20C

decreases from about 10 (1) millions in the 1970s to about 250,000 prior the 1930 [see *Poli et al*., 2015, Figure 14]. The effects of this considerable change in the observational network on the long-term climate trends reproduced in ERA-20C have been widely discussed by *Poli et al.* [2013, 2015]. The results presented here suggest that the representation of the synoptic midlatitude atmospheric variability can be affected as well. In other words, the scarce coverage of observations available may be insufficient to support and feed high-frequency disturbances in the reanalysis for the first part of the century, leading to disruption of the "natural" high-frequency disturbances present in the model and therefore to reduced high-frequency variability. This can be conceptually understood considering a wave-like disturbance (or simply a moving sine wave). A model with the correct climatological characteristics will produce a wave of the right amplitude and phase speed but, in general, not the correct phase. If observations are plentiful, they will simply ensure the phase is correct. However, scattered rare observations would be problematic. It would do nothing (in the absence of observation error) if the phase happened by chance to be correct but would simply hamper the disturbance if the phase was out by 180°, and the observation was at the trough or crest of the real wave. The single observation would either reduce the amplitude of the crest in the model background, leaving the trough unaffected, or would reduce the amplitude of the trough in the model background, leaving the crest unaffected. The (small) number of observations in the early twentieth century affects the synoptic variability in 20CR as well. In the earlier decades 3-D fields such as Z500 are systematically characterized by a larger ensemble spread (Figure 5S), mostly over Pacific Ocean where the underestimation of synoptic variability in the first decades of the twentieth century is more evident (Figure 3). This enlarged ensemble spread is an indication of a more pronounced internal variability due to the "scarse observational constraint" of the 56 Kalman filter ensemble runs. Therefore, the underestimation of synoptic variability exhibited by 20CR is most likely due to the smoothing induced by the 56-member mean. In the recent period, since surface observations are denser, all the 56 solutions are constrained toward the real state of the atmosphere with less dispersion. This translates in a reduced spread and consequently in a more realistic synoptic variability in the ensemble mean. Other papers have already discussed the limitations in 20CR in describing the synoptic variability before 1950, since spurious and nonphysical trends are present [*Wang et al*., 2012; *Krueger et al*., 2014, 2013].

In both twentieth century reanalysis products the suppression of high-frequency variability during the first decades of the century seems to be due to low data coverage and should not be incorrectly interpreted as a climate signal. These results suggest to motivate further the data rescue of in situ historical observational records. Lastly, the methodology developed in the present study can serve to benchmark the synoptic quality of forthcoming model simulations and reanalyses.

Acknowledgments

This work has been supported by the EU-FP7 2007–2013 project SPECS (308378). Susanna Corti acknowledges the NCAS Visiting Scientist Programme for supporting her work. The comments of an anonymous referee and F. Chauvin contributed to a notable improvement to this paper. The data sets ERA-20CM, ERA-20C, ERA-Interim, and ERA-40 data are available on a public server at http://apps.ecmwf.int/datasets/. The ensemble mean and ensemble spread of NOAA Twentieth Century Reanalysis, as well as NCEP reanalysis, are freely available in NOAA ftp server ftp.cdc.noaa.gov. The data sets ERA-20CM-SP and the codes used to compute Hayashi spectra are available on request to authors.

References

Benzi, R., and A. Speranza (1989), Statistical properties of low-frequency variability in the Northern Hemisphere, *J. Clim.*, *2*, 367–379, doi:10.1175/1520-0442(1989).

Benzi, R., P. Malguzzi, A. Speranza, and A. Sutera (1986), The statistical properties of general atmospheric circulation: Observational evidence and a minimal theory of bimodality, *Q. J. R. Meteorol. Soc.*, *112*, 661–674, doi:10.1002/qj.49711247306.

Blackmon, M. (1976), A climatological spectral study of 500 mb geopotential height of Northern Hemisphere, *J. Atmos. Sci.*, *33*, 1607–1623, doi:10.1175/1520-0469(1976).

Charney, J., and D. Straus (1980), Form-drag instability, multiple equilibria and propagating planetary waves in baroclinic, orographically forced, planetary wave systems, *J. Atmos. Sci.*, *37*(6), 1157–1176.

Charney, J., and J. De Vore (1979), Multiple flow equilibria in the atmosphere and blocking, *J. Atmos. Sci.*, *36*, 1205–1216, doi:10.1175/1520-0469(1979)036.

Compo, G. P., J. S. Whitaker, and P. D. Sardeshmukh (2006), Feasibility of a 100-year reanalysis using only surface pressure data, *Bull. Am. Meteorol. Soc.*, *87*, 175–190.

Compo, G. P., et al. (2011), The Twentieth Century Reanalysis Project, *Q. J. R. Meteorol. Soc.*, *137*, 1–28, doi:10.1002/QJ.776.

Dee, D. P., et al. (2011), The ERA-Interim reanalysis: Configuration and performance of the data assimilation system, *Q. J. R. Meteorol. Soc.*, *137*, 553–597.

Dell'Aquila, A., V. Lucarini, P. Ruti, and S. Calmanti (2005), Hayashi spectra of the Northern Hemisphere mid-latitude atmospheric variability in the NCEP-NCAR and ECMWF reanalyses, *Clim. Dyn.*, *25*, 1639–652, doi:10.1007/s00382-005-0048-x.

Di Biagio, V., S. Calmanti, A. Dell'Aquila, and P. M. Ruti (2014), Northern Hemisphere winter midlatitude atmospheric variability in CMIP5 models, *Geophys. Res. Lett.*, *41*, 1277–1282, doi:10.1002/2013GL058928.

Fraedrich, K., and H. Bottger (1978), A wavenumber frequency analysis of the 500 mb geopotential at 50°N, *J. Atmos. Sci.*, *35*, 745–750.

Hayashi, Y. (1971), A generalized method for resolving disturbances into progressive and retrogressive waves by space Fourier and time cross-spectral analysis, *J. Meteorol. Soc. Jpn.*, *49*, 125–128.

Hayashi, Y. (1979), A generalized method of resolving transient disturbances into standing and travelling waves by space-time spectral analysis, *J. Atmos. Sci.*, *36*, 1017–1029, doi:10.1175/1520-0469(1979)036<1017:AGMORT>2.0.CO;2.

Hersbach, H., C. Peubey, A. Simmons, P. Berrisford, P. Poli, and D. Dee (2015), ERA-20CM: A twentieth-century atmospheric model ensemble, *Q. J. R. Meteorol. Soc.*, doi:10.1002/QJ.2528.

Kistler, R., et al. (2001), The NCEP-NCAR 50-year reanalysis: Monthly means CD-ROM and documentation, *Bull. Am. Meteorol. Soc.*, *82*(2), 247–267.

Krueger, O., F. Schenk, F. Feser, and R. Weisse (2013), Inconsistencies between long-term trends in storminess derived from the 20cr reanalysis and observations, *J. Clim.*, *26*(3), 868–874, doi:10.1175/JCLI-D-12-00309.1.

Krueger, O., F. Feser, L. Bärring, E. Kaas, S. To, H. Tuomenvirta, and S. Hans (2014), Comment on "Trends and low frequency variability of extra-tropical cyclone activity in the ensemble of twentieth century reanalysis" by Xiaolan L. Wang, Y. Feng, G. P. Compo, V. R. Swail, F. W. Zwiers, R. J. Allan, and P. D. Sardeshmukh, Climate Dynamics, 2012, *Clim. Dyn.*, *42*, 1127–1128.

Lucarini, V., S. Calmanti, A. Dell'Aquila, P. M. Ruti, and A. Speranza (2007), Intercomparison of the Northern Hemisphere winter midlatitude atmospheric variability of the IPCC models, *Clim. Dyn.*, *28*, 829–848, doi:10.1007/s00382-006-0213-x.

Palmer, T., R. Buizza, F. Doblas-Reyes, T. Jung, M. Leutbecher, J. Shutts, G. M. Steinheimer, and A. Weisheimer (2009), Stochastic parametrization and model uncertainty, Tech. Memo. 598, Eur. Cent. for Medium- Range Weather Forecasts, Reading, U. K.

Poli, P., et al. (2013), The data assimilation system and initial performance evaluation of the ECMWF pilot reanalysis of the 20th-century assimilating surface observations only (ERA-20C) ECMWF ERA Report Series 14, ECMWF, Shinfield Park, Reading.

Poli, P., H. Hersbach, P. Berrisford, D. Dee, A. Simmons, and P. Laloyaux (2015), ERA-20C deterministic. ECMWF ERA Report Series 20, ECMWF, Shinfield Park, Reading.

Rayner, N. A., D. E. Parker, E. B. Horton, C. K. Folland, L. V. Alexander, D. P. Rowell, E. C. Kent, and A. Kaplan (2003), Global analyses of sea surface temperature, sea ice, and night marine air temperature since the late nineteenth century, *J. Geophys. Res.*, *108*(D14), 4407, doi:10.1029/2002JD002670

Ruti, P., V. Lucarini, A. Dell'Aquila, S. Calmanti, and A. Speranza (2006), Does the subtropical jet catalyze the midlatitude atmospheric regimes?, *Geophys. Res. Lett.*, *33*, L06814, doi:10.1029/2005GL024620.

Speranza, A. (1983), Deterministic and statistical properties of the westerlies, *Pure Appl. Geophys.*, *121*, 511–562, doi:10.1007/BF02590154.

Taylor, K. E., R. J. Stouffer, and G. A. Meehl (2012), An overview of cmip5 and the experiment design, *Bull. Am. Meteorol. Soc.*, *93*, 485–498, doi:10.1175/BAMS-D-11-00094.1.

Thépaut, J.-N. (2006), Assimilating only surface-pressure observations in 3- and 4D-Var, in *Proceedings of ECMWF/GEO Workshop on Atmospheric Re-analysis*, ECMWF, Reading, UK.

Uppala, S. M., et al. (2005), The ERA-40 re-analysis, *Q. J. R. Meteorol. Soc.*, *131*, 2961–3012, doi:10.1256/qj.04.176.

Wallace, J., S. Tibaldi, and A. Simmons (1983), Reduction of systematic forecast errors in the ECMWF model through the introduction of an envelope orography, *Q. J. R. Meteorol. Soc.*, *109*, 683–717, doi:10.1002/QJ.49710946202.

Wang, X. L., Y. Feng, G. P. Compo, V. R. Swail, F. W. Zwiers, R. J. Allan, and P. D. Sardeshmukh (2012), Trends and low frequency variability of extra-tropical cyclone activity in the ensemble of twentieth century reanalysis, *Clim. Dyn.*, doi:10.1007/s00382-012-1450-9.

Weisheimer, A., S. Corti, T. Palmer, and F. Vitart (2014), Addressing model error through atmospheric stochastic physical parameterisations: Impact on the coupled ECMWF seasonal forecasting system, *Philos. Trans. R. Soc. A*, *372*, doi:10.1098/rsta.2013.0290.

Whitaker, J. S., G. P. Compo, and J. N. The´paut (2009), A comparison of variational and ensemble-based data assimilation systems for reanalysis of sparse observations, *Mon. Weather Rev.*, *137*, 1991–1999, doi:10.1175/2008MWR2781.1.